Supporting Information

Single-Atom Bi Embedded in the Surface Lattice of Pd Nanoparticles: Enhancing Catalytic Activity and Stability for Formic Acid Dehydrogenation

Jianfei Jin,[a] Dongqin Guo,[a] Zhichao Liu,[ab] Hui Yin,[ab] Niangxiu Li,[ab] Aiming Zhang,[ab] Feng Liu,[ab] Yunbo Jiang,*[ab]

[a]State Key Laboratory of Precious Metal Functional Materials, Kunming Institute of Precious Metals, Kunming, China
[b]Yunnan Precious Metals Laboratory Co., Ltd., Kunming, China

Correspondence: Yunbo Jiang (E-mail: jyb@ipm.com.cn)

Supplementary Note

According to the previous studies, the hydrogen production rate r for the aqueous formic acid formate solution can be expressed as follows at the steady state [1]:

$$r = \frac{kb_{f,M}c_f}{[1 + b_{f,M}c_f + (b_{f,B}c_f)^{0.5} + (b_H c_H)^{0.5}]^2} \qquad \text{(S1)}$$

where k denotes the kinetic rate constant, c_{f} and c_{H} denote the concentrations of formate ion and dihydrogen in the solution. $b_{\mathrm{f,M}}$ $b_{\mathrm{f,B}}$ and b_{H} are the adsorption constants of HCOO∗ M, HCOO∗ B and H* respectively.Where * denotes an active site, HCOO∗ M and HCOO∗ B denotes the formate species occupying one and two active sites, respectively. Notably, the cleavage of the C−H in HCOO∗ M bond is a kinetically essential step of FAD, whereas HCOO∗ B serves as a spectator species due to a very high energy barrier for the cleavage of its H−C bond. Equation S1 suggests that a maximum r can be obtained by varying c_f, which is consistent with previous reports [1,2].

Based on DFT, the effect of Bi atom doping on the catalytic decomposition of formic acid on the Pd(111) surface was systematically investigated. By calculating the adsorption energies of reactants, reaction intermediates, and products, as well as the activation barriers of transition states, the regulatory mechanism of Bi doping on the reactivity of the Pd(111) surface was elucidated. First, the adsorption behaviors of key species such as HCOOH, COOH, HCOO, and CO_2 were examined. As shown in Figure S6, these species all exhibit a bidentate coordination mode, interacting with surface Pd atoms through C–Pd, O–Pd, or H–Pd bonds. Specifically, HCOOH coordinates via its O and H atoms, HCOO forms covalent bonds with surface Pd through its two O atoms, while COOH and CO_2 bond with Pd atoms via one C atom and one O atom.

In this work, Bi_1@Pd/CMK-3 refers to 0.08Bi@Pd/CMK-3; FA refers to formic acid and SF refers to sodium formate.

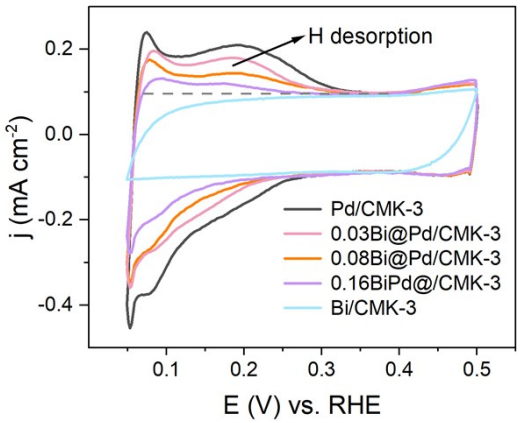

Figure S1. Cyclic voltammograms displaying hydrogen adsorption-desorption for Pd/CMK, 0.03Bi@Pd/CMK, 0.08Bi@Pd/CMK-3, 0.16Bi@Pd/CMK, and Bi/CMK-3 in 0.1 M $HClO_4$ at 10 mV s^{-1}

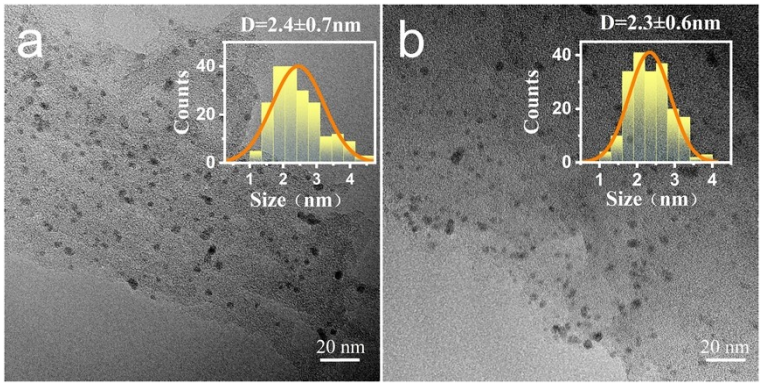

Figure S2. TEM images and corresponding statistical distribution of the particle sizes of (A) Pd/CMK and (B) Bi_1@Pd/CMK-3 after 3 cycles of catalytic FAD in 1.1 M FA + 2.4 M SF solution at 323 K

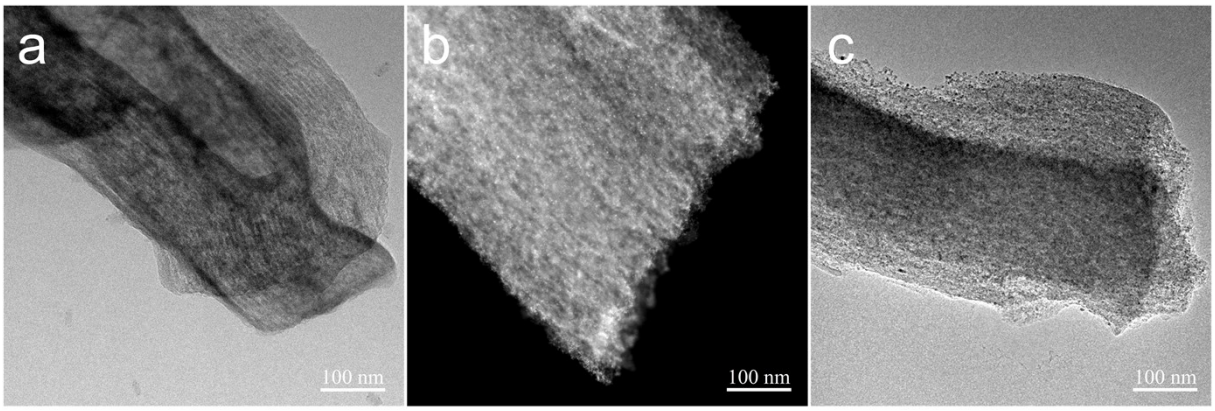

Figure S3. TEM image of (A) CMK-3, (B) HAADF-STEM image of Bi_1@Pd/CMK-3, (C) TEM image of Bi_1@Pd/CMK-3 after 300h FAD

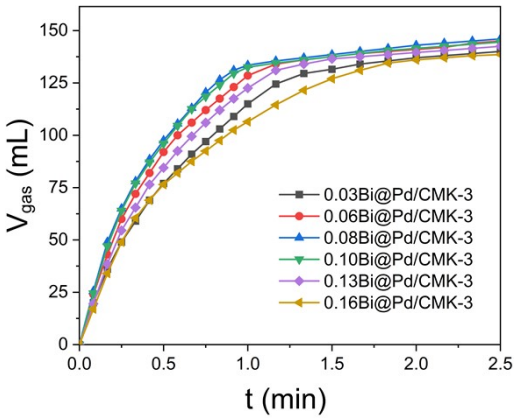

Figure S4. Time course of gas evolution from 2 mL of 1.1 M FA + 2.4 M SF solution in the presence of 32 mg of *x*Bi@Pd/C at 323 K with different Bi/Pd molar ratio *x*

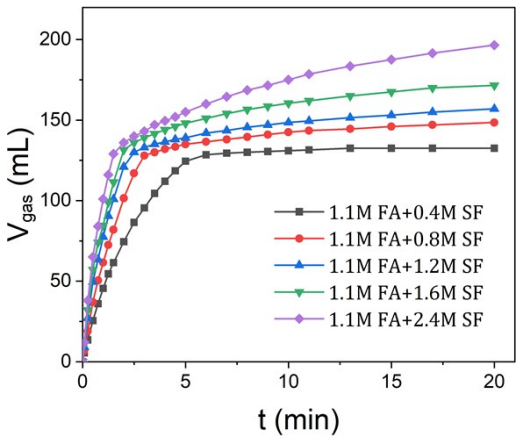

Figure S5. Time course of gas evolution from 2 mL of 1.1 M FA + n M SF solution with 32 mg of Pd/CMK-3 at 323 K

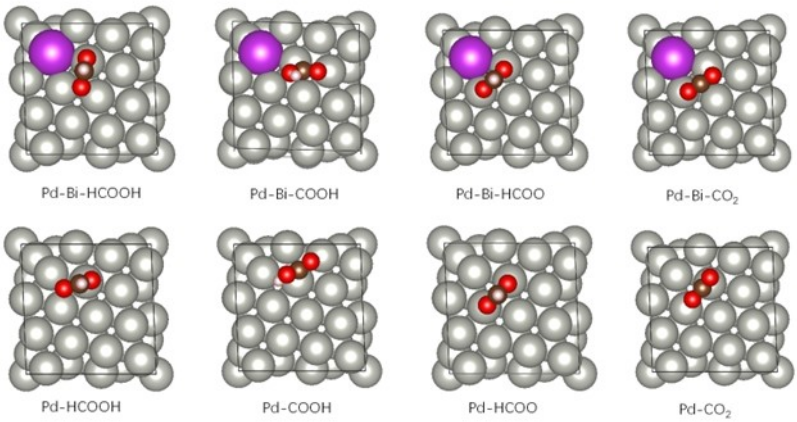

Figure S6. Adsorption configurations of HCOOH, COOH, HCOO, and CO_2 on Bi_1@Pd-(111) and Pd(111) surfaces.

Precursor Pd wt%	Measured Pd wt%	Measured n_{Bi}/n_{Pd}, *x*
5.00	4.97	0.00
4.96	4.83	0.08
4.93	4.93	0.16
5.00	4.47	0.00(300h-FAD)
4.96	4.68	0.08(300h-FAD)

Table S1. Pd deposition on Pd/C and *x*Bi@Pd/CMK-3 measured by ICP-AES.

Precursor Bi wt%	Measured Bi wt%	Precursor n_{Bi}/n_{Pd} *x*
0.294	0.294	0.03
0.586	0.587	0.06
0.779	0.775	0.08
0.972	0.977	0.10
1.069	1.085	0.11
1.260	1.257	0.13
1.547	1.503	0.16
0.584	0.775	0.08(without Pd)
0.779	0.734	0.08(300h-FAD)

Table S2. Bi deposition on Pd/CMK-3 and *x*Bi@Pd/CMK-3 measured by ICP-AES.

Table S3. TOF of Catalytic formic acid dehydrogenation at 323 K with different concentration of sodium formate in 2 mL aqueous solution.

Catalyst	c_{FA} (mol L^{-1})	c_{SF} (mol L^{-1})	TOF (h^{-1})
Pd/CMK-3	1.1	0.4	3226
	1.1	0.8	4857
	1.1	1.2	6555
	1.1	1.6	8334
	1.1	2.4	9919
	1.1	3.2	11447
	1.1	4.0	12355
	1.1	4.8	11662
Bi_1@Pd/CMK-3	1.1	0.4	6498
	1.1	0.8	10319
	1.1	1.2	13425
	1.1	1.6	15799
	1.1	2.4	19762
	1.1	3.2	22620
	1.1	4.0	24012
	1.1	4.8	21028

Table S4. TOF values of catalytic formic acid dehydrogenation performed over different catalysts in different conditions - a comparison with literature reports.

Catalyst	Temperature (℃)	c_{FA} (mol L^{-1})	c_{SF} (mol L^{-1})	TOF(h^{-1})	Reference
Bi_1@Pd/CMK-3	30	1.1	2.4	7275	This work
	40			12827	
	50			19762	
	60			28902	
	30	1.1	0.8	3556	
	50			10320	
Pd/CMK-3	50	1.1	2.4	9919	This work
$PdBi_{0.11}$/C	30	1.1	2.4	4350	[1]
Pd-N30 /C	30	1.1	0.8	3481	[3]
Pd/CN_{ZM}	50	1.0	1.0	4157	[4]
Pd/NH_2-CNT	30	0.5	2.0	2560	[5]
	50			8137	
Pd/FeNC	50	1.5	3.75	7361	[6]
$Pd_{60}Au_{40}$/HPC-NH_2	25	2.5	0	3763	[7]
Pd/YSMSNs-NH_2(10-3)	50	0.5	1	2783	[8]
In situ-Pd@MSC	30	3.6	3.6	2569	[9]
	50			6700	
Pd–WO_x/(P)NPCC	30	0.5	1.5	2877	[10]
	50			6135	
Pd-B/C	30	1.1	0.8	1184	[11]
$Au_{0.4}Pd_{0.6}$/PEI-PDA@CNCs	50	0.5	2	4258	[12]
	60			7159	

$Pd_{0.6}Co_{0.2}Ni_{0.2}$/N-CN	25	0.5	0.5	1249	[13]
Pd/NHPC-AC	60	1.5	1.5	4115	[14]
Ag_2Pd_8/TiO_2-M-450	60	1.5	4.5	4789	[15]
AP-SiO_2@PDA-NGO@Pd	50 65	1.06	0	8274 18625	[16]

References

[1] X. Qin, H. Li, S. Xie, K. Li, T. Jiang, X.-Y. Ma, K. Jiang, Q. Zhang, O. Terasaki, Z. Wu and W.-B. Cai, ACS Catalysis, 2020, 10, 3921-3932.

[2] Q. Wang, N. Tsumori, M. Kitta and Q. Xu, ACS Catalysis, 2018, 8, 12041-12045.

[3] Y. Yu, X. Wang, C. Liu, F. Vladimir, J. Ge and W. Xing, Journal of Energy Chemistry, 2020, 40, 212-216.

[4] M. Deng, A. Yang, J. Ma, C. Yang, T. Cao, S. Yang, M. Yao, F. Liu, X. Wang and J. Cao, ACS Applied Materials & Interfaces, 2022, 14, 18550-18560.

[5] Y. Kim, H. Lee, S. Yang, J. Lee, H. Kim, S. Hwang, S. W. Jeon and D. H. Kim, Journal of Catalysis, 2021, 404, 324-333.

[6] S. Zhong, X. Yang, L. Chen, N. Tsumori, N. Taguchi and Q. Xu, ACS Applied Materials & Interfaces, 2021, 13, 46749-46755.

[7] Z. Wang, S. Liang, X. Meng, S. Mao, X. Lian and Y. Wang, Applied Catalysis B: Environmental, 2021, 291, 120140.

[8] C. Zhou, S. Li, H. Chai, Q. Liu, J. Hu, Z. Liu, K. Yu, F. Fan, W. Zhou, A. Duan, C. Xu and X. Wang, Applied Catalysis B: Environment and Energy, 2024, 346, 123750.

[9] Q.-L. Zhu, F.-Z. Song, Q.-J. Wang, N. Tsumori, Y. Himeda, T. Autrey and Q. Xu, Journal of Materials Chemistry A, 2018, 6, 5544-5549.

[10] A. Zhang, J. Xia, Q. Yao and Z.-H. Lu, Applied Catalysis B: Environmental, 2022, 309, 121278.

[11] K. Jiang, K. Xu, S. Zou and W.-B. Cai, Journal of the American Chemical Society, 2014, 136, 4861-4864.

[12] J. Shen, Y. Liang, C. Wang and Y. Zhu, Chemical Engineering Journal, 2023, 473, 144640.

[13] Z. Dong, F. Li, Q. He, X. Xiao, M. Chen, C. Wang, X. Fan and L. Chen, International Journal of Hydrogen Energy, 2019, 44, 11675-11683.

[14] Y. Chen, X. Li, Z. Wei, S. Mao, J. Deng, Y. Cao and Y. Wang, Catalysis Communications, 2018, 108, 55-58.

[15] X. Sun, F. Li, Z. Wang, H. An, W. Xue and Y. Wang, ChemCatChem, 2021, 14, e202101528.

[16] W. Ye, W. Pei, S. Zhou, H. Huang, Q. Li, J. Zhao, R. Lu, Y. Ge and S. Zhang, Journal of Materials Chemistry A, 2019, 7, 10363-10371.